Acta Cryst B
STRUCTURAL SCIENCE
CRYSTAL ENGINEERING
MATERIALS
ISSN 2052-5206

# Meta-generalized gradient approximation time-dependent density functional theory study of electron trapping in Hf- and Zr-doped lutetium oxide: influencing the oxygen vacancy

**Andrii Shyichuk***

Faculty of Chemistry, University of Wrocław, 14 F. Joliot-Curie, Wrocław, Lower Silesia 50-383, Poland.
*Correspondence e-mail: andrii.shyichuk@uwr.edu.pl

Received 12 May 2023
Accepted 4 September 2023

Edited by P. Macchi, Politecnico di Milano, Italy

**Keywords:** thermoluminescence; meta-generalized gradient approximation; meta-GGA; time-dependent density-functional theory; TD-DFT; trap depth; storage phosphors.

**Supporting information**: this article has supporting information at journals.iucr.org/b

This work analyzes the effects of a nearby Hf or Zr dopant on the electron density trapped at an oxygen vacancy site. The two metals are among the dopants used to achieve thermoluminescence and energy storage in phosphors based on cubic lutetium oxide (c-$Lu_2O_3$). The presence of oxygen vacancies is anticipated in those phosphors. If the dopant is located outside the immediate surroundings of the vacancy site, the resulting optical trap depth is similar to that of the isolated oxygen vacancies (1.6–1.7 eV versus 1.7 eV). If the dopant is one of the four metal cations surrounding the vacancy site, the corresponding trap depth is 2.0–2.1 eV. Using time-dependent density-functional theory calculations, it was found that the excitation of the vacancy-trapped electrons can take two forms: a local excited state at the vacancy site can be formed, or an electron transfer to Hf might occur. With charge compensation in mind, several structures with three defects were analyzed: the dopant cation, the vacancy and an interstitial oxygen (Hf/Zr plus a Frenkel pair). These last two systems with the dopant in a +4 oxidation state and a single electron trapped at the vacancy site correspond to zero total charge, while another electron can be trapped. The vacancy site is expected to trap the electron, not the dopant. The composite defects of the dopant and Frenkel pair are thus considered the most likely electron traps in cubic $Lu_2O_3$:Hf and cubic $Lu_2O_3$:Zr.

## 1. Introduction

Cubic lutetium oxide (c-$Lu_2O_3$) materials doped with Tb or Pr may, upon excitation, exhibit charge carrier trapping, the corresponding long-term energy storage and, consequently, thermoluminescence. Defects or dopants capable of electron trapping (typically transition metals of the *d* block) must be introduced in order to achieve such properties. The lanthanide is considered to be the hole trap and the recombination center. Depending on the electron trap depth, afterglow or long-term (permanent) energy storage can be achieved. The positions of thermoluminescence glow curve peaks (that is, the temperatures of maximum emission intensity at a given heating rate) depend strongly on the impurities responsible for it, as well as on the respective trap depth (Zych *et al.*, 2017; Kulesza *et al.*, 2018; Bolek *et al.*, 2019).

Previously, electron trapping in $Lu_2O_3$:Ta has been attributed [using density functional theory, (DFT) calculations] to the dopant cations (Shyichuk & Zych, 2019), which was in line with the available experimental data and semi-empirical vacuum-referred binding energy model [known as the Dorenbos model (Dorenbos, 2017)]. In another example, the depth of the oxygen vacancy localized electron trap was found to be consistent with experimental estimates (Shyichuk &

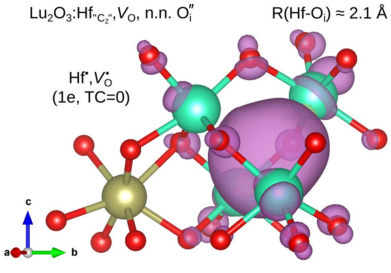

Zych, 2020). However, the case of $Lu_2O_3$:Hf happened to be not that straightforward. In particular, the Hf-localized electron in $Lu_2O_3$:Hf corresponds to either a low-energy trap of 0.8 eV at most, or no trapping at all, depending on the particular dopant ion arrangements (Shyichuk *et al.*, 2022). In the latter paper, the same computational approach was used to analyze several kinds of Hf-based electron traps, and only a few of them were found to be sufficiently deep to explain the observed glow peaks, although those required two dopant ions to sit on the second-nearest-neighbor sites. That paper also provides a detailed introduction, where the glow peaks of different Hf-codoped $Lu_2O_3$ are compared.

Briefly, $Lu_2O_3$:Pr,Hf samples usually exhibit several glow curve peaks at very distinct temperatures, namely at about 135°C, 250°C and 340°C, the middle one being the most prominent (Wiatrowska & Zych, 2012, 2013*a*,*b*). Further studies indicated that the main peak might also be split in two at about 200°C and 270°C (Kulesza *et al.*, 2013), or it may be shifted slightly to about 230°C, while a fourth peak appears at about 300°C (Kulesza *et al.*, 2016). In $Lu_2O_3$:Tb,Hf, the main glow peak is located at about 240–260°C, with a lower-intensity shoulder ending at about 350°C (Sójka *et al.*, 2019; Kulesza *et al.*, 2018, 2016, 2010, 2013; Kulesza & Zych, 2013). The peak positions may depend quite significantly on the heating rate (Zych & Kulesza, 2014). A feature common to both Tb and Pr co-doped samples is a small (fading with time) peak at about 70–150°C. Another common feature is the main peak, mostly occurring at about 240–260°C. The estimated trap depths of about 1.6–1.7 eV for this peak correspond quite well to the *in silico* value of the oxygen vacancy electron trap depth (estimated using DFT; Shyichuk & Zych, 2020). Three peaks with shapes and proportions similar to those of $Lu_2O_3$:Pr,Hf also occur in $Lu_2O_3$:Tb,Sr and $Lu_2O_3$:Tb,Ba (Trojan-Piegza *et al.*, 2009), where the co-dopants are the non-luminescent alkali earth cations. The low-temperature (∼130°C) peak is the only one present in $Lu_2O_3$:Tb,Sr (Chen *et al.*, 2012).

Given the similarities in glow peaks between Hf co-doped materials and those where oxygen vacancies are anticipated (Trojan-Piegza *et al.*, 2009; Chen *et al.*, 2012), it is likely that at least some of the former are actually caused by the vacancies. With that idea in mind, for the present work several structures containing both oxygen vacancies and Hf dopant located at several different distances were analyzed. Additionally, systems with Hf dopant and a Frenkel pair (oxygen vacancy plus interstitial oxygen) were considered. The most representative of the defects were also analyzed with Zr instead of Hf. In agreement with the experimental data, the two cations exhibited very similar values for the trap depths. While tempting, no comparison of the results with the experimental data has been done, as such a comparison would have been unsafe. Some of the found traps are similar in depth to that of the isolated oxygen vacancy (obtained via the same DFT-based approach).

All of the analyzed structures resulted in electron traps of moderate depth, where the trapped electrons were located at the vacancy site. With charge compensation considered, the most likely candidate for the electron trapping is the composite defect $Lu_2O_3:Hf^{\bullet}, V_O^{\bullet}, O_i''$ (that is, an $Hf^{4+}$ ion, an interstitial $O^{2-}$ and a single electron trapped at $V_O$) – a charge-neutral system with a single trapped electron, which is capable of deep-trapping another electron. The same is true for the analogous Zr-based composite defect. For these defects, the effect of the distance between the $V_O$ and $O_i$ sites was investigated. Time-dependent DFT (TD-DFT) was applied to analyze the excitation of the trapped electrons. Kröger–Vink notation (Kröger & Vink, 1956) is used in this paper.

## 2. Experimental

The calculations followed the approach described in previous work on the subject (Shyichuk & Zych, 2019, 2020; Shyichuk *et al.*, 2022). The refined experimental structure of cubic $Lu_2O_3$ from Zeler *et al.* (2014) has been optimized with *Quantum Espresso* (Giannozzi *et al.*, 2009, 2017) using the Perdew–Zunger (Perdew & Zunger, 1981) local density approximation (LDA PZ) exchange-correlation functional and GBRV ultrasoft pseudopotentials (Garrity *et al.*, 2014). A plane-wave cutoff of 40–42 Ry was used (depending on the structure) and the *k*-point grid was 3×3×3. The optimized cell was subjected to defect creation and the resulting structures were optimized again. All-electron calculations followed, using the full-potential linearized augmented plane wave (FP-LAPW) (Wimmer *et al.*, 1981) in the augmented plane wave with local orbitals flavor (APW+lo+LO in *Wien2k* notation; Blaha *et al.*, 2020). The RPP meta-generalized gradient approximation (Räsänen *et al.*, 2010) exchange and LDA PZ correlation density functionals were utilized. The all-electron calculations were single-point energy calculations [resulting in density of states (DOS) and magnetization density], on top of which TD-DFT (Sharma *et al.*, 2012, 2011) calculations followed. Please refer to the supporting information for full details.

## 3. Results and discussion

### 3.1. Cell size and bond lengths

The introduction of $Hf^{4+}$ into the $Lu_2O_3$ structure resulted in slight decrease in the size of the latter. The introduction of both $Hf^{4+}$ and a $V_O^{\times}$ (an oxygen vacancy with two electrons in it) does not result in much of a cell-size change compared with the $Hf^{4+}$-only structure (namely, a 0.01% increase). A similar result was obtained previously without Hf (Shyichuk & Zych, 2020). Also in this case, the two electrons in the oxygen vacancy do not cause any significant distortions with respect to the structure without a vacancy (with the oxygen ion in its regular position). The relative positions of Hf and $V_O^{\times}$ have virtually no effect on this behavior. From Table 1, it is clear that the distance between Hf and the oxygen vacancy in the $Lu_2O_3:M,V_O$ system has a negligible effect on the unit-cell volume. Zr doping, however, results in slightly smaller cells than in the Hf-doped analogues. Note that in $Lu_2O_3:M,V_O,O_i$, the differences between the Zr- and Hf-doped systems are much smaller.

**Table 1**
The effects of the analyzed defects on the unit-cell size of $Lu_2O_3$.

'Exp.' refers to experimentally obtained data (Zeler *et al.*, 2014), and 'Calc.' refers to calculations made using the method described in this paper.

| $R_0$(Hf–$V_O$) (Å, label) | Impurities $M$ and symmetry | Cell charge | No. of trapped electrons | High spin | $R(M$–$V_O)$ (Å) | $R(M$–$O_i)$ (Å) | $R(V_O$–$O_i)$ (Å) | Cell volume (Å$^3$) | $\Delta V_{cell}$ (%) relative to $Lu_2O_3$ | | $\Delta V_{cell}$ (%) relative to $Lu_2O_3$:$X$ | |
|---|---|---|---|---|---|---|---|---|---|---|---|---|
| | | | | | | | | | Exp. | Calc. | $X = V_O$ | $X = Hf^{4+}$ |
| 2.215 | Zr, $V_O$, $C_{3i}$ | 1 | 2 | No | 2.23 | | | 1071.06 | −1.56 | −0.51 | −0.52 | −0.06 |
| 2.215 | Hf, $V_O$, $C_{3i}$ | 1 | 2 | No | 2.19 | | | 1073.11 | −1.49 | −0.44 | −0.46 | 0.00 |
| 4.05 | | 1 | 2 | No | 4.31 | | | 1073.25 | −1.49 | −0.44 | −0.45 | 0.01 |
| 4.195 | | 1 | 2 | No | 4.13 | | | 1073.40 | −1.48 | −0.43 | −0.45 | 0.01 |
| 4.585 | | 1 | 2 | No | 4.32 | | | 1073.38 | −1.49 | −0.43 | −0.45 | 0.01 |
| 6.723 | | 1 | 2 | No | 6.70 | | | 1073.30 | −1.49 | −0.44 | −0.45 | 0.01 |
| 4.195 | | 1 | 2 | No | 4.13 | | | 1073.40 | −1.49 | −0.43 | −0.45 | 0.01 |
| 4.195 | | 1 | 2 | Forced | 4.12 | | | 1074.12 | −1.46 | −0.41 | −0.43 | 0.03 |
| 4.195 | Zr, $V_O$, $C_{3i}$ | 1 | 2 | No | 4.12 | | | 1070.72 | −1.57 | −0.52 | −0.53 | −0.07 |
| 4.195 | Zr, $V_O$, $O_i$, $C_{3i}$ | 0 | 1 | Yes | 4.12 | 2.02 | 4.39 | 1089.85 | −0.98 | 0.07 | 0.06 | 0.52 |
| 4.195 | Hf, $V_O$, $O_i$, $C_{3i}$ | 0 | 1 | Yes | 4.13 | 2.07 | 4.40 | 1092.18 | −0.91 | 0.14 | 0.13 | 0.59 |
| | | −1 | 2 | No | 4.14 | 2.08 | 4.42 | 1104.10 | −0.55 | 0.51 | 0.49 | 0.96 |
| | | −1 | 2 | Forced | 4.13 | 2.08 | 4.42 | 1105.29 | −0.52 | 0.54 | 0.53 | 0.99 |
| | | −2 | 3 | Yes | 4.14 | 2.09 | 4.44 | 1118.22 | −0.13 | 0.93 | 0.92 | 1.39 |
| | | 0 | 1 | Yes | 4.15 | 5.44 | 7.49 | 1093.83 | −0.86 | 0.20 | 0.18 | 0.64 |
| | | −1 | 2 | No | 4.16 | 5.46 | 7.54 | 1105.76 | −0.50 | 0.56 | 0.54 | 1.01 |
| | | −1 | 2 | Forced | 4.16 | 5.45 | 7.53 | 1106.56 | −0.48 | 0.58 | 0.57 | 1.03 |
| | | −2 | 3 | Yes | 4.21 | 5.47 | 7.57 | 1119.19 | −0.10 | 0.96 | 0.95 | 1.41 |
| 4.195 | Zr, $V_O$, $O_i$, $C_{3i}$ | 0 | 1 | Yes | 4.14 | 5.43 | 7.48 | 1091.34 | −0.94 | 0.12 | 0.11 | 0.57 |
| 2.180 | Zr, $V_O$, $C_2$ | 1 | 2 | No | 2.41 | | | 1071.20 | −1.55 | −0.50 | −0.52 | −0.05 |
| 2.180 | Hf, $V_O$, $C_2$ | 1 | 2 | No | 2.38 | | | 1072.98 | −1.50 | −0.45 | −0.46 | 0.00 |
| 3.866 | | 1 | 2 | No | 3.99 | | | 1073.29 | −1.49 | −0.44 | −0.45 | 0.01 |
| 4.088 | | 1 | 2 | No | 4.36 | | | 1073.13 | −1.49 | −0.44 | −0.46 | 0.00 |
| 4.334 | | 1 | 2 | No | 4.45 | | | 1073.10 | −1.49 | −0.44 | −0.46 | 0.00 |
| 6.782 | | 1 | 2 | No | 6.49 | | | 1073.25 | −1.49 | −0.44 | −0.45 | 0.01 |
| 4.241 | | 1 | 2 | No | 4.04 | | | 1073.25 | −1.49 | −0.44 | −0.45 | 0.01 |
| 4.241 | Zr, $V_O$, $C_2$ | 1 | 2 | No | 4.04 | | | 1070.65 | −1.57 | −0.52 | −0.53 | −0.07 |
| 4.241 | Zr, $V_O$, $O_i$, $C_2$ | 0 | 1 | Yes | 4.01 | 2.03 | 4.40 | 1089.57 | −0.99 | 0.07 | 0.05 | 0.52 |
| 4.241 | Hf, $V_O$, $O_i$, $C_2$ | 0 | 1 | Yes | 4.01 | 2.09 | 4.41 | 1092.06 | −0.92 | 0.14 | 0.13 | 0.59 |
| | | −1 | 2 | No | 4.03 | 2.10 | 4.43 | 1103.97 | −0.56 | 0.50 | 0.49 | 0.95 |
| | | −1 | 2 | Forced | 4.04 | 2.10 | 4.44 | 1105.26 | −0.52 | 0.54 | 0.53 | 0.99 |
| | | −2 | 3 | Yes | 4.06 | 2.11 | 4.45 | 1118.01 | −0.14 | 0.93 | 0.91 | 1.38 |
| | | 0 | 1 | Yes | 4.05 | 5.88 | 7.49 | 1093.78 | −0.87 | 0.19 | 0.18 | 0.64 |
| | | −1 | 2 | No | 4.07 | 5.90 | 7.54 | 1105.67 | −0.51 | 0.56 | 0.54 | 1.00 |
| | | −1 | 2 | Forced | 4.08 | 5.89 | 7.54 | 1106.41 | −0.49 | 0.58 | 0.56 | 1.03 |
| | | −2 | 3 | Yes | 4.10 | 5.92 | 7.59 | 1119.59 | −0.09 | 0.98 | 0.96 | 1.43 |
| 4.241 | Zr, $V_O$, $O_i$, $C_2$ | 0 | 1 | Yes | 4.05 | 5.88 | 7.48 | 1091.34 | −0.94 | 0.12 | 0.11 | 0.57 |

The introduction of interstitial oxygen $O_i$ in addition to $Hf^{4+}/Zr^{4+}$ and a $V_O^{\times}$ (total cell charge −1) results in about a 1% increase in the cell volume compared with the $Hf^{4+}$-only structure. The $Lu_2O_3:Hf^{\bullet}, V_O^{\bullet}, O_i''$ structure (where only one electron is trapped) is 0.64% larger than the $Hf^{4+}$-only structure ($Lu_2O_3:Hf^{\bullet}$). The $Lu_2O_3:M,V_O,O_i$ systems with a single trapped electron exhibit cell volumes most closely similar to that of pure $Lu_2O_3$. In other words, the $Lu_2O_3:M^{\bullet}, V_O^{\bullet}, O_i''$ systems exhibit the lowest structural distortions within the studied set, with only 0.1–0.2% deviation from the undoped cell size.

The introduction of additional electrons results in a noticeable cell expansion of about half a percent for each added electron. A forced high-spin state (resulting in the vacancy electrons being unpaired) results in negligible changes in the cell volume with respect to the low-spin ground state.

In Table 1 and the following text, the values of $R_0(M$–$V_O)$ are shown. These are the distances between the $M$ = Zr/Hf dopant site and the oxygen vacancy site (the removed oxygen) in the defect-free structure. This particular labeling is selected due to the fact that the respective post-optimization values depend on the charge state of the system. $R_0$ is a more intuitive label than the (much more abstract) number of the oxygen position in the initial geometry, *e.g.* O51. Despite these changes, $R_0$ still reflects the trends (or, in most cases, the complete lack of such whatsoever).

### 3.2. The $Hf^{\bullet}$-$V_O^{\times}$ system

Oxygen vacancies have a strong tendency to be formed in c-$Lu_2O_3$, as was deduced from various pieces of experimental evidence [see Shyichuk & Zych (2020) and references therein, Petermann *et al.* (2002) in particular]. The present work has analyzed whether an Hf dopant could have any effect on a nearby oxygen vacancy. An empty oxygen vacancy ($V_O^{\bullet\bullet}$) is characterized by a local charge of +2, corresponding to a missing oxygen anion. A cluster with $Hf^{4+}$ ($Hf^{\bullet}, V_O^{\bullet\bullet}$) is then +3

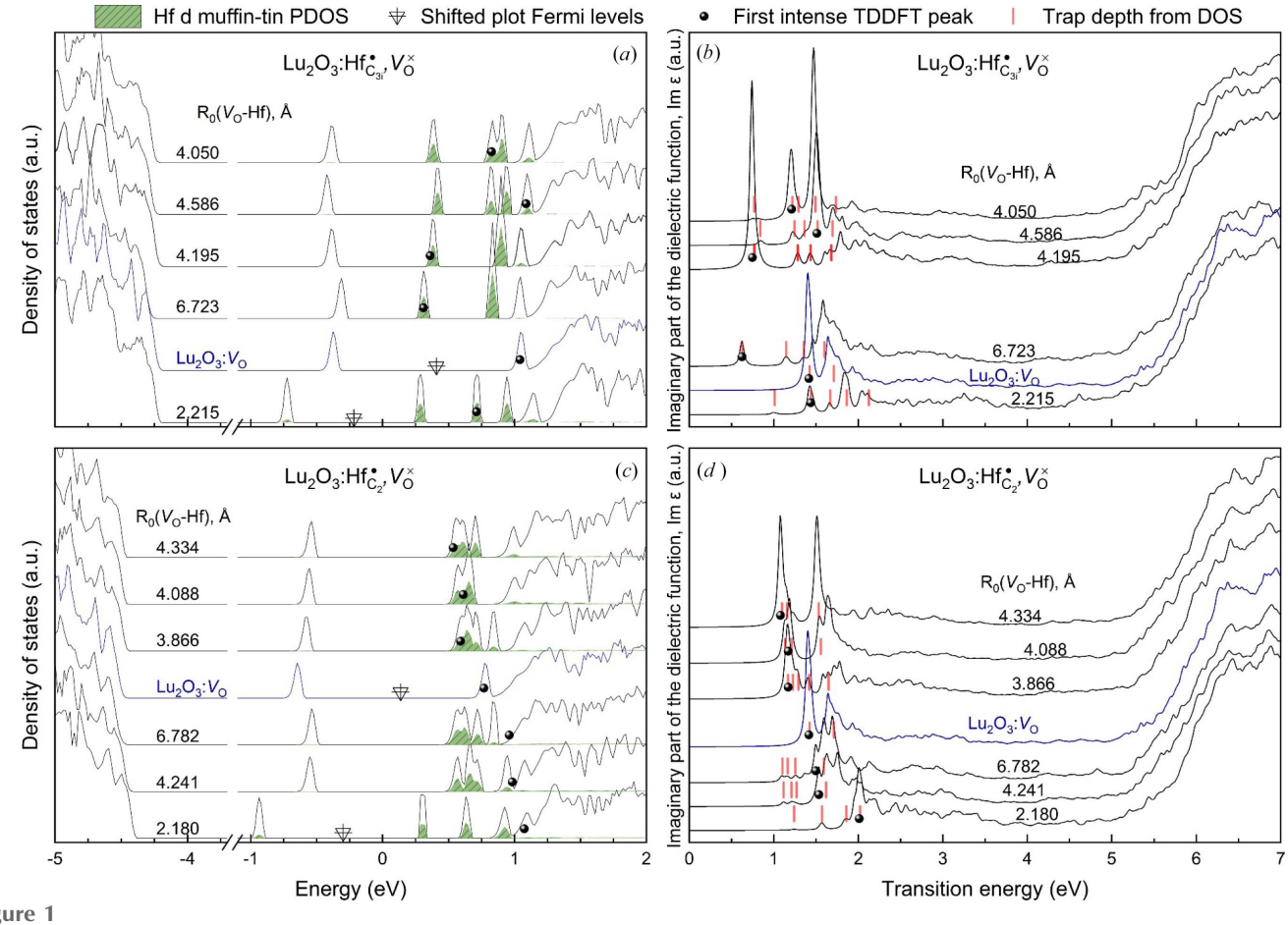


**Figure 1**
(*a*) and (*c*) DOS and (*b*) and (*d*) optical absorption (imaginary part of the dielectric function from TD-DFT) for $Lu_2O_3:Hf^{\bullet}, V_O^{\times}$. In panels (*a*) and (*c*) the Fermi level is at zero or at the triangular markers. Trap depths are calculated from the DOS, assuming electron transfer to the conduction band or the lower defect bands.

charged, which is quite high. Such a charge, however, can be compensated with *e.g.* an $Lu^{3+}$ vacancy, which has been assumed to be lying outside the studied cell (roughly 10 Å or more from the Hf site) and is not modeled explicitly. Another possibility involves an interstitial $O^{2-}$, which is considered below in the following sections of this paper.

A series of samples where an oxygen vacancy was located in proximity to an Hf dopant was analyzed. First, samples with total charge of +3 ($Lu_2O_3:Hf^{\bullet}, V_O^{\bullet\bullet}$, empty traps) were considered. The dopant was kept on either the $C_{3i}$ or $C_2$ Lu site, while different oxygen atoms (selected to be approximately the same distance from the dopant on either of the sites) were removed to create an oxygen vacancy. For both metal sites, one of the options included Hf in the immediate vicinity of the vacancy: an oxygen bound to the dopant (the one common to the two sites) was removed (see the supporting information). In the DOS plots, several trap states below the conduction band were found. Thus, the study moved to the next step, where samples with a total charge of +1 ($Lu_2O_3:Hf^{\bullet}, V_O^{\times}$) were analyzed, corresponding to the vacancy holding two paired trapped electrons.

In $Lu_2O_3:Hf^{\bullet}, V_O^{\times}$, the Hf ion remains in its +4 oxidation state, while the vacancy trap is full (doubly occupied). Such a conclusion is drawn from the DOS (Fig. 1) and radial electron density plots (Fig. 2). In particular, the peak located about 0.5 eV below the Fermi level is free from Hf 5*d* contributions and is also present in the $Lu_2O_3:V_O^{\times}$ plots (Fig. 1). The radial probability (likelihood of finding the electron at a certain distance) plots (Fig. 2) indicate that the corresponding eigenvalue electron density is most abundant between 0 and 2 Å from the vacancy site. The density associated with the lowest trap band is closely confined on the vacancy site, almost identically to the isolated vacancy case (Shyichuk & Zych, 2020). The Hf 5*d* muffin-tin density contributions to the trapped electron density are close to zero. In augmented plane wave calculations, muffin-tin spheres are atom-centered non-overlapping spheres, inside of which the basis is atomic orbital-like, while the plane waves fill the interstitial space. Here, the Zr sphere radius was 2.2 Bohr, while the Hf sphere radius was 2.3 Bohr. In the case of Hf being a member of the vacancy surroundings, there is a slightly larger contribution of Hf density, albeit still small.

In the DOS plots of $Lu_2O_3:Hf^{\bullet}, V_O^{\times}$ (Fig. 1), the Hf bands can be distinguished from the vacancy bands by the partial DOS plots of the Hf 5*d* muffin-tin sphere electron density [the filled part of the plots in panels (*a*) and (*c*)]. The first peak above the Hf bands is the upper peak of the oxygen vacancy $V_O^{\bullet}$ (Shyichuk & Zych, 2020), which sometimes overlaps with

**Table 2**
Trap depth of the $Lu_2O_3:Hf^{\bullet}$, $V_O^{\times}$ systems.

The minimal gap is the energy difference between the occupied oxygen vacancy state and the next empty band above it. Entries in *italics* are comparisons of Zr and Hf dopants.

| Structure | Vacancy site | $R_0(V_O$–Hf) (Å) | Trap depth (eV) | Minimal gap (eV) |
|---|---|---|---|---|
| $Lu_2O_3:Hf^{\bullet}_{C_{3i}}, V_O^{\times}$ | O51 | 2.215 | *2.13* | *1.01* |
| $Lu_2O_3:Zr^{\bullet}_{C_{3i}}, V_O^{\times}$ | O51 | 2.215 | *1.99* | *0.73* |
| $Lu_2O_3:Hf^{\bullet}_{C_{3i}}, V_O^{\times}$ | O71 | 4.050 | 1.74 | 0.77 |
| $Lu_2O_3:Hf^{\bullet}_{C_{3i}}, V_O^{\times}$ | O61 | 4.195 | 1.68 | 0.77 |
| $Lu_2O_3:Hf^{\bullet}_{C_{3i}}, V_O^{\times}$ | O64 | 4.195 | 1.68 | 0.77 |
| $Lu_2O_3:Hf^{\bullet}_{C_{3i}}, V_O^{\times}$ | O43 | 4.585 | 1.70 | 0.84 |
| $Lu_2O_3:Hf^{\bullet}_{C_{3i}}, V_O^{\times}$ | O52 | 6.723 | *1.60* | *0.63* |
| $Lu_2O_3:Zr^{\bullet}_{C_{3i}}, V_O^{\times}$ | O52 | 6.723 | *1.67* | *0.62* |
| $Lu_2O_3:Hf^{\bullet}_{C_2}, V_O^{\times}$ | O51 | 2.180 | *2.02* | *1.24* |
| $Lu_2O_3:Zr^{\bullet}_{C_2}, V_O^{\times}$ | O51 | 2.180 | *1.87* | *1.02* |
| $Lu_2O_3:Hf^{\bullet}_{C_2}, V_O^{\times}$ | O61 | 3.866 | 1.65 | 1.17 |
| $Lu_2O_3:Hf^{\bullet}_{C_2}, V_O^{\times}$ | O43 | 4.088 | 1.56 | 1.13 |
| $Lu_2O_3:Hf^{\bullet}_{C_2}, V_O^{\times}$ | O64 | 4.241 | 1.62 | 1.12 |
| $Lu_2O_3:Hf^{\bullet}_{C_2}, V_O^{\times}$ | O71 | 4.334 | 1.53 | 1.10 |
| $Lu_2O_3:Hf^{\bullet}_{C_2}, V_O^{\times}$ | O52 | 6.782 | *1.59* | *1.10* |
| $Lu_2O_3:Zr^{\bullet}_{C_2}, V_O^{\times}$ | O52 | 6.782 | *1.64* | *0.89* |
| $Lu_2O_3:V_O^{\times}$ | O35 | | 1.71 | 1.42 |

**Table 3**
Trap depth of the $Lu_2O_3:M^{\bullet}$, $V_O^{\times}$, $O_i''$ systems.

| System | $O_i$ position | Cell charge | Trap depth (eV) |
|---|---|---|---|
| $Lu_2O_3:Zr^{\bullet}_{C_{3i}}, V_O^{\bullet}, O_i''$ | Bound to Zr/Hf | 0 | 2.17 |
| $Lu_2O_3:Hf^{\bullet}_{C_{3i}}, V_O^{\bullet}, O_i''$ | | 0 | 2.17 |
| $Lu_2O_3:Hf^{\bullet}_{C_{3i}}, V_O^{\times}, O_i''$ | | −1 | 1.45 |
| $Lu_2O_3:Hf^{\bullet}_{C_{3i}}, V_O', O_i''$ | | −2 | 1.50 |
| $Lu_2O_3:Zr^{\bullet}_{C_{3i}}, V_O^{\bullet}, O_i''$ | Distant | 0 | 2.22 |
| $Lu_2O_3:Hf^{\bullet}_{C_{3i}}, V_O^{\bullet}, O_i''$ | | 0 | 2.20 |
| $Lu_2O_3:Hf^{\bullet}_{C_{3i}}, V_O^{\times}, O_i''$ | | −1 | 1.68 |
| $Lu_2O_3:Hf^{\times}_{C_{3i}}, V_O^{\times}, O_i''$ | | −2 | 1.58 |
| $Lu_2O_3:Zr^{\bullet}_{C_2}, V_O^{\bullet}, O_i''$ | Bound to Zr/Hf | 0 | 2.13 |
| $Lu_2O_3:Hf^{\bullet}_{C_2}, V_O^{\bullet}, O_i''$ | | 0 | 2.14 |
| $Lu_2O_3:Hf^{\bullet}_{C_2}, V_O^{\times}, O_i''$ | | −1 | 1.57 |
| $Lu_2O_3:Hf^{\bullet}_{C_2}, V_O', O_i''$ | | −2 | 1.53 |
| $Lu_2O_3:Zr^{\bullet}_{C_2}, V_O^{\bullet}, O_i''$ | Distant | 0 | 2.19 |
| $Lu_2O_3:Hf^{\bullet}_{C_2}, V_O^{\bullet}, O_i''$ | | 0 | 2.19 |
| $Lu_2O_3:Hf^{\bullet}_{C_2}, V_O^{\times}, O_i''$ | | −1 | 1.55 |
| $Lu_2O_3:Hf^{\bullet}_{C_2}, V_O', O_i''$ | | −2 | 1.61 |

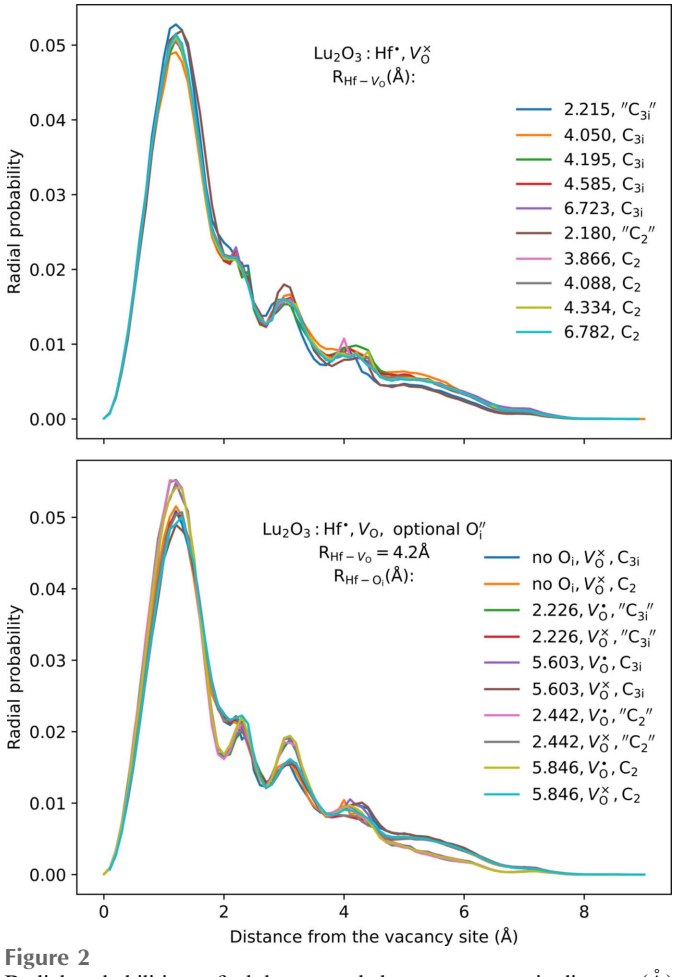


**Figure 2**
Radial probabilities to find the trapped electron at a certain distance (Å) from the vacancy barycenter, for the systems with (lower part) and without (upper part) the interstitial oxygen. The $V_O^{\times}$ plots are from Γ-point wavefunction plots, while the $V_O^{\bullet}$ plots are from magnetization densities.

the conduction band. From the three-dimensional electron density plots [not shown here, but discussed in the previous work (Shyichuk *et al.*, 2022)], the bands with a strong Hf contribution correspond to Hf-localized states that exhibit *d*-orbital shapes. The occupied band (below the Fermi level) at about −0.5 eV is the filled oxygen vacancy trap. It is clear that the Hf bands lie much closer to the conduction band than to the vacancy band. This would make the corresponding (Hf-localized) electron traps much more shallow than the oxygen vacancy trap. The deepest Hf traps are about half the depth of the $V_O^{\times}$ trap. While it might be unsafe to compare the trap depths from these calculations directly with the experimental glow curve values (Shyichuk & Zych, 2019), this conclusion originates from the calculated data comparison, which is legitimate.

As can be seen from the DOS plots in Figs. 1(*a*) and 1(*c*) and from Table 2, the $V_O^{\times}$ trap depth is only slightly influenced by the presence of Hf dopant at proximity. The exception happens when Hf is part of the vacancy coordination surroundings, resulting in a much deeper trap. In the selected cases, structures with a Zr dopant were also analyzed and compared with the respective Hf counterparts. The respective values are emphasized in Table 2 in *italic* font. The trap depths are very similar, especially for the larger Hf—$V_O$ distance. The differences in the depths are non-zero though, and would be detectable using thermoluminescence techniques. According to Table 3, adding an interstitial oxygen to the system results in a slight reduction in the trap depth for the two-electron trap (systems with total charge −1).

In order to check the $V_O^{\times}$ trap optical depth, time-dependent DFT (TD-DFT) calculations were performed. As the vacancy band is the highest occupied band, it was assumed that the TD-DFT excitations would mostly happen from there to the higher (empty) bands. The vertical red lines in Figs. 1(*b*) and 1(*d*) visualize the optical trap depths estimated from the DOS as band–band energy differences. There is a clear correspon-

dence between the DOS peaks and the TD-DFT peak positions, meaning that the (optical) trap depth estimation from the DOS [as described by Shyichuk & Zych (2020)] corresponds well to the TD-DFT optical absorption peaks.

For each sample, the most intense TD-TDF transition energy is marked in Figs. 1(*b*) and 1(*d*). The same mark is placed on the corresponding DOS plots, at the position defined as the oxygen vacancy band position plus the transition energy. In such a way the transition character can be estimated from the DOS, using its energy and assuming the oxygen vacancy band as the initial state. Some of the intense peaks thus correspond to $V_O^{\times} \rightarrow Hf^{\bullet}$. The most prominent observations here are the differences in the TD-DFT absorption character of the samples. The intensities of the $V_O^{\times} \rightarrow Hf^{\bullet}$ transitions (which can be identified as such via comparison of the respective transition energies with the energy differences from the DOS) are slightly different among the samples. There is no clear correlation between the $V_O^{\times}-Hf^{\bullet}$ distance and the TD-DFT absorption character. However, as seen from these calculations, the presence of Hf in proximity to a filled oxygen vacancy trap in $Lu_2O_3$ might influence its optical depth (optically stimulated electron release energy/wavelength) in some cases.

### 3.3. Trapped electron localization

Localization of the trapped electrons was analyzed using three-dimensional plots of the respective densities. For the spin-unpolarized systems with two trapped electrons, this was the Γ-point wavefunction plot for the Kohn–Sham (KS) eigenvalue corresponding to the trapped electron band. For the spin-polarized systems, this was the total magnetization density. While wavefunction plots in *Elk* (https://elk.sourceforge.io) are limited to a particular *k*-point, magnetization plots characterize the system as a whole. Moreover, for systems with unpaired electrons, a spatial magnetization plot is a natural way of finding the localization of the unpaired electron density. In *Elk* , the wavefunction plot is always a single electron density. It can thus be directly compared with the magnetization density of a single unpaired electron. In Fig. 2, such a comparison is made in terms of radial probability plots, which are the integral probabilities of finding the electron in a spherical shell approximately 0.1 Å thick. The values for such plots were calculated as an integral density in the voxels situated *R* (Å) from the vacancy barycenter, where *R* was rounded to one decimal place and the periodic boundary was taken into account. The barycenter was taken to lie on the averaged coordinate of the four cations surrounding the vacancy.

From Fig. 2, it is clear that no matter the system, the plots look essentially the same as the plot corresponding to an isolated oxygen vacancy in lutetium oxide (Shyichuk & Zych, 2020). Most of the density is located less than 2 Å from the barycenter. The minor peaks correspond to the positions of the surrounding ions: the four cations (at about 2.5 Å), the first layer of oxygens (at about 3 Å) and the second shell of

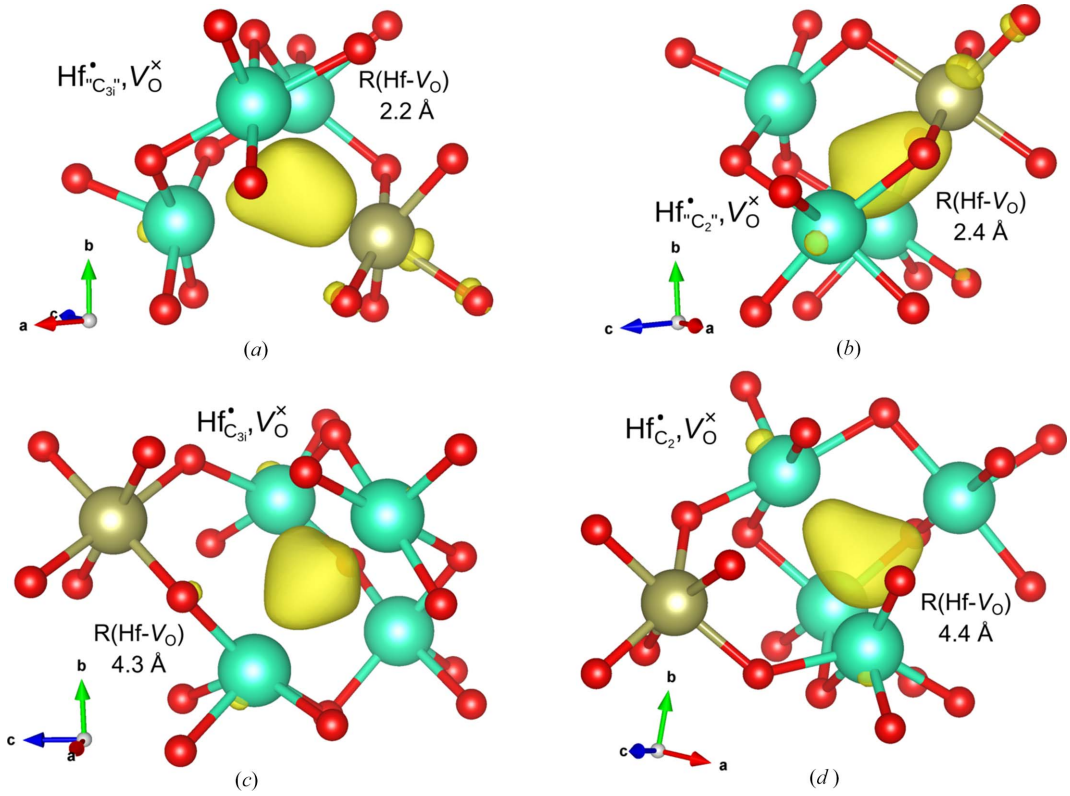


**Figure 3**
Wavefunction plots corresponding to the trapped electron KS eigenvalues at the Γ-point. The isosurface level is 0.006. Lu atoms are turquoise, O atoms red and Hf golden. Hf is either part of the immediate surround of the vacancy (*a*), (*b*), or located in the second coordination sphere (*c*), (*d*).

metal cations (at about 4 Å). The same is true for either one or two electrons situated on the vacancy site. The changes in trap depths observed in Table 1 must thus (probably) originate from electrostatic interaction between the trapped electron density and the $Hf^{4+}$ cation, and do not originate from the changes in the trapped electron density shape.

Noteworthy examples are the systems where $Hf^{4+}$ is one of the four cations surrounding the vacancy site. The corresponding trap depths are 2.0–2.1 eV, while in the other cases the depths are 1.6–1.7 eV. The changes in distance between the Hf site and the vacancy site have a rather minor effect on the trap depth. However, placing the Hf dopant in the vicinity of the vacancy results in a significant increase in the trap depth (Table 2). The radial distribution of the densities remains the same, despite the fact that the densities are spatially shifted towards Hf [Figs. 3(*a*) and 3(*b*)]. Without Hf in the direct surroundings of the vacancy, the density is spread rather equally between the four Lu atoms [Figs. 3(*c*) and 3(*d*)]. Note that the $Lu_4$ surroundings correspond to a spatially smaller blob than the $Lu_3Hf$ surroundings (Fig. 3). In other words, in the $Lu_4$ neighborhood the electrons trapped at the vacancy are less delocalized and have more interstitial character, while in the $Lu_3Hf$ neighborhood the atomic (localized) contribution from Hf is larger (note the smaller blobs at Hf on the side opposite from the vacancy). It can be concluded that the participation of Hf orbitals in delocalization of the trapped electron density results in the increased trap depth.

The isosurface plots shown in Figs. 3, 5 and 6 are visualizations of *Elk* 3D plots. In *Elk*, the integral over the cell can be approximated by summing the values of the 3D output file, dividing by the total number of points in the file and multiplying by the unit-cell volume. Thus, the integral is approximated by multiplication of the sum by the voxel volume of the 3D plot. The sum is about 170 with a $109\times109\times109$ data grid. The units of the isosurface are thus the unitary electron localization probability (dimensionless) divided by the voxel volume, or the reciprocal voxel volume. The values could have been reintegrated to unity, but were kept 'as is' for improved reproducibility.

### 3.4. Systems with $O_i$

While the Hf,$V_O$ systems have provided some valuable insights, the formation of those particular defects is questionable. With two trapped electrons, the net uncompensated charge on the former two-species defect is +1, which should promote formation of an interstitial oxygen rather than an oxygen vacancy. If the trap is empty, the uncompensated charge is +3 – again positive and thus promoting the inclusion of additional anions. In the reducing atmosphere commonly used in the synthesis of $Lu_2O_3$-based thermoluminescent materials (Kulesza *et al.*, 2016), Hf dopant in a +3 oxidation state can form, with the following Frenkel pair formation:

$$Lu_2O_3:Hf^{\times} \rightarrow Lu_2O_3:Hf^{\times}, V_O^{\bullet\bullet}, O_i'' \rightarrow Lu_2O_3:Hf^{\bullet}, V_O^{\bullet}, O_i'',$$

with a redox sub-reaction of $Hf^{\times} + V_O^{\bullet\bullet} \rightarrow Hf^{\bullet} + V_O^{\bullet}$, where the electron from Hf is transferred to the empty vacancy site. A few Hf-doped systems with an interstitial oxygen anion and an oxygen vacancy (*i.e.* with a Frenkel pair) were thus considered.

In those cases where Hf was not part of the surroundings of the vacancy site, its role in electron trapping needed to be clarified. For that, a few structures were selected where the Hf—$V_O$ distance was about 4.2 Å, meaning that Hf was a member of the second-nearest shell of the cations with respect to the vacancy site. An optional interstitial oxygen was added either to the Hf coordination surroundings or distant from both Hf and $V_O$ (5–6 Å from Hf in particular). In these structures, the presence of $O_i$ and its position were the variables. The number of trapped electrons was changed as well. In the charge-neutral $Lu_2O_3:Hf^{\bullet}, V_O^{\bullet}, O_i''$ system with a semi-occupied oxygen vacancy trap, the vacancy eigenstate is singly occupied. In the overpopulated $Lu_2O_3:Hf', V_O^{\times}, O_i''$/$(Lu_2O_3:Hf^{\bullet}, V_O^{\times}, O_i'')'$ systems, the vacancy site is doubly occupied and the additional electron has to occupy the higher levels. Those can be either localized Hf 5*d* states or the delocalized bands (Shyichuk *et al.*, 2022). The corresponding DOS plots are shown in Fig. 4.

**3.4.1. Systems with $O_i$: DOS plots**. All of the DOS plots in Fig. 4 share similar features: an Hf-free peak below the Fermi level (corresponding to the vacancy), bands of Hf character (that can be distinguished by the respective partial DOS of the muffin-tin fraction of Hf 5*d* atomic electron density) and some interstitial oxygen bands immediately above the valence band. The attribution of the latter was discussed in our previous work on the matter (Shyichuk *et al.*, 2022).

Figs. 4(*b*), 4(*f*), 4(*j*) and 4(*n*) contain two sets of DOS plots, both corresponding to $Lu_2O_3:Hf^{\bullet}, V_O^{\times}, O_i''$. Those labeled LS are low-spin, as expected for a doubly occupied single-eigenvalue electron trap. Those labeled FHS correspond to the forced high-spin (FHS, triplet) states, where magnetization (corresponding to two unpaired electrons per cell) was enforced. One of the trapped electrons may remain in the vacancy KS state/band, while the other one is forbidden to do so by Pauli exclusion as both electrons have their spins 'up'. The second electron must thus occupy the lowest unoccupied KS state/band, which may or may not have (at least some) Hf character. The purpose of the FHS calculation was to check whether the excited electron would occupy Hf states (localize at Hf). Among the tested cases, the only one where that happens is $Lu_2O_3:Hf_{C_{3i}}, V_O^{\bullet}, O_i''$ (FHS) with the $O_i$ distant from Hf [Fig. 4(*f*)]. For the rest of the structures, where $O_i$ is part of the dopant surroundings, or the dopant is on the $C_2$ site, the excited electron occupies the second (higher-energy, band-like) state (Shyichuk & Zych, 2020) related to the vacancy. In Figs. 4(*b*), 4(*j*) and 4(*n*), the Hf-related bands in the FHS plots lie right above the respective Fermi level (shown with a triangular marker, not at zero). The FHS peaks right below the Fermi level for these three plots are Hf-free.

Other than the FHS calculation, no set of starting parameters and geometries was found to result in a trapped electron localization at Hf with either an empty or a semi-filled vacancy band. The electrons would (eventually) always end up in the vacancy trap and not in the Hf trap – at least when both

defects fit within a single unit cell. Such a result is not surprising: the vacancy bands are lower in energy than the Hf bands, and accordingly the former get populated. It was concluded that Hf cannot act as an independent electron trap in proximity to the oxygen vacancy trap.

**3.4.2. Systems with an $O_i$: TD-DFT.** Another aspect of the study was the role of the Hf bands in excitation of the trapped electron density. From Fig. 1 it was clear that, in some cases, a sharp, intense peak in the TD-DFT optical absorption prediction corresponded to a transition from the vacancy band

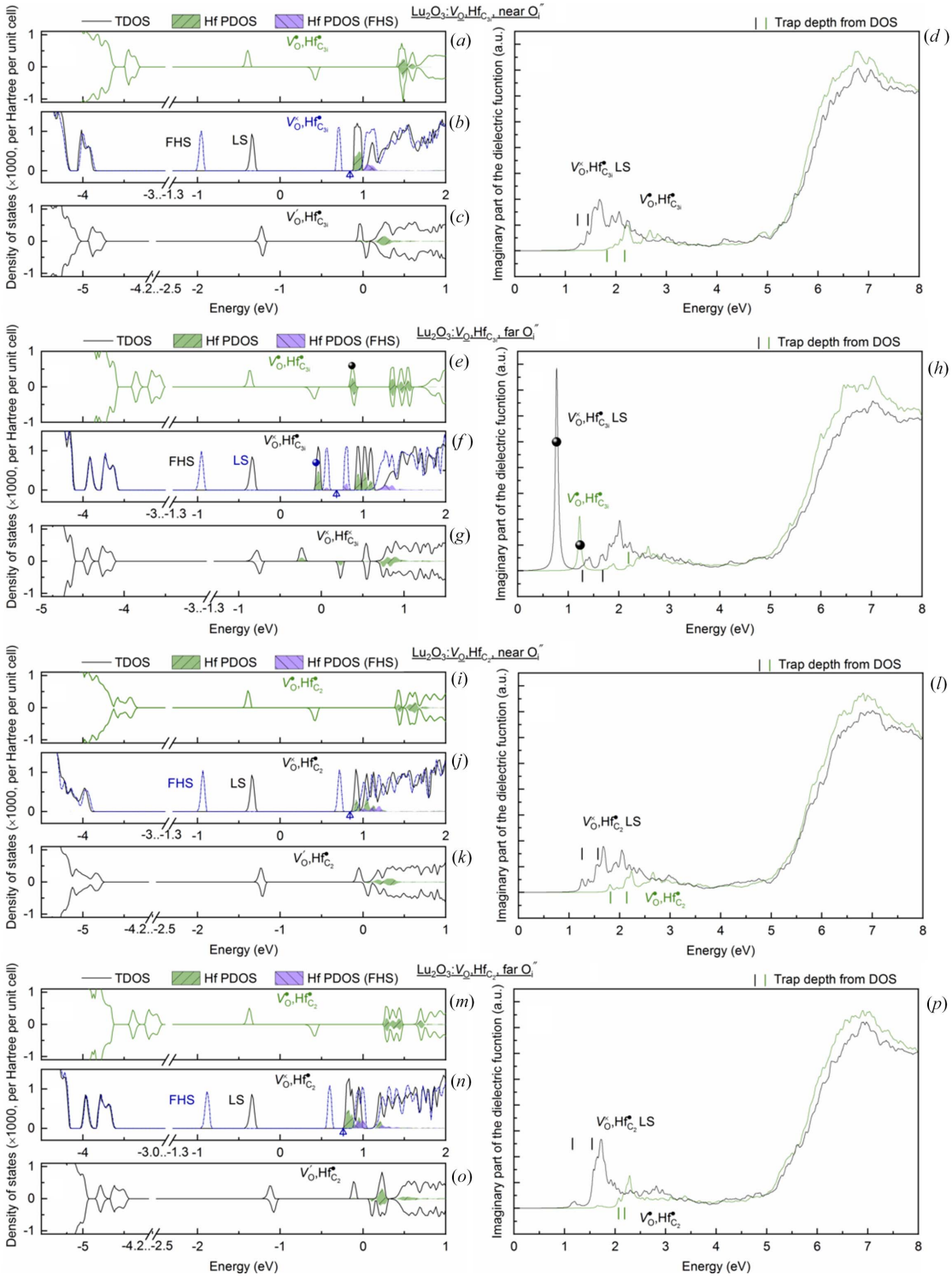


**Figure 4**
(*a*)–(*c*), (*e*)–(*g*), (*i*)–(*k*) and (*m*)–(*o*) DOS and (*d*), (*h*), (*l*) and (*p*) simulated optical absorption (imaginary part of the dielectric function from TD-DFT) for $Lu_2O_3$:$Hf^{\bullet}$, $V_O$, $O_i''$. In the DOS plots, the Fermi level is at zero or at the triangular markers. Trap depths are calculated from the DOS, assuming electron transfer to the conduction band or the lower defect bands.

to an Hf-character band, while for some other systems a sharp peak was not observed. The question was: what would the corresponding excited-state electron density look like? The structures corresponding to the Fig. 4 plots shared the $V_O$ location and differed in the Hf site, while the Hf—$V_O$ distance differed only slightly between the structures. With such a setup, the differences in the absorption (and in the excited-state) properties can be mostly attributed to the change in Hf site symmetry, and not to the change in the Hf—$V_O$ distance.

Figs. 4(*d*), 4(*h*), 4(*l*) and 4(*p*) exhibit the simulated optical absorption profiles (the imaginary part of the dielectric function) for the four $Lu_2O_3:Hf^{\bullet}, V_O, O_i''$ samples. The vertical bars in these plots correspond to the trap depths calculated from the DOS. It is clear that the depths correspond well to the lower-energy part of the optical absorption peaks; the depths are thus estimates of the optical trap depths. The $Lu_2O_3:Hf^{\bullet}, V_O^{\bullet}, O_i''$ systems are characterized by deeper traps (and higher energy absorption bands) than the $Lu_2O_3:Hf^{\bullet}, V_O^{\times}, O_i''$ systems, while the band-gap edge absorption starts at about 5 eV for both. Only the $Lu_2O_3:Hf_{C_{3i}}, V_O, O_i''$ system is characterized by sharp spikes in the absorption [Fig. 4(*h*)]. The position of these spikes corresponds perfectly to the energy of a $V_O^{\times/\bullet} \rightarrow Hf^{\bullet}$ transition [as defined from the DOS, Figs. 4(*e*) and 4(*f*)]. In this very system, the FHS calculation results in a one-electron population of the shallow Hf trap. Apparently, the absorption

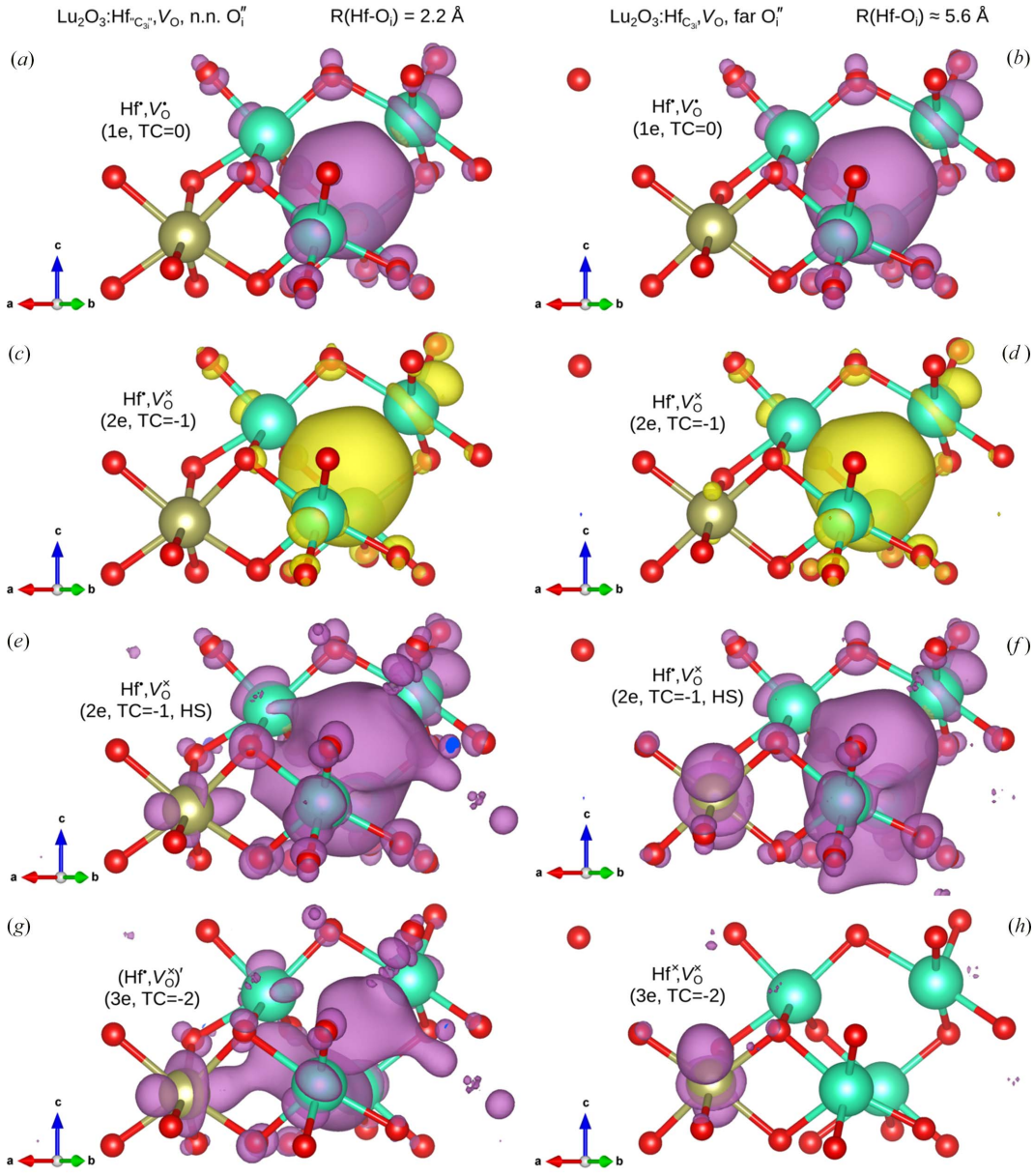


**Figure 5**
(*a*), (*b*), (*e*)–(*h*) Magnetization plots and (*c*) and (*d*) isosurface plots of the wavefunction corresponding to the trapped-electron KS eigenvalues at the Γ-point for $Lu_2O_3:Hf_{C_{3i}}, V_O, O_i''$ with different numbers of additional/trapped electrons. The isosurface level is 0.0015. Lu atoms are turquoise, O atoms red, Hf golden.

spikes must result from $V_O^{\times/\bullet} \rightarrow Hf^{\bullet}$ electron transfer. In the rest of the $Lu_2O_3:Hf^{\bullet}, V_O, O_i''$ systems, the FHS state does not include Hf and the spikes are not present.

**3.4.3. Systems with an $O_i$: electron localization.** In order to analyze the character of trapped electron localization in the $Lu_2O_3:Hf^{\bullet}, V_O, O_i''$ systems, the spatial distribution of the corresponding magnetization was analyzed (Figs. 5 and 6). For the closed-shell $Lu_2O_3:Hf^{\bullet}, V_O^{\times}, O_i''$ systems, wavefunction plots (electron densities corresponding to the vacancy KS eigenvalues) were calculated [Figs. 5(*c*), 5(*d*), 6(*c*) and 6(*d*)]. In subplots (*a*)–(*d*) of both figures, the blobs of electron/magnetization densities look very similar: the magnetization density of one trapped electron and the electron density of two trapped electrons look spatially the same, which is expected as they correspond to the same band (KS eigenvalue). In the *Elk* software, both kinds of densities are computed as single-electron and are thus directly comparable.

The magnetization densities of the two-trapped-electrons FHS state [Figs. 5(*e*), 5(*f*), 6(*e*) and 6(*f*)] look distinctly different: they occupy a much larger volume and spread out to numerous atoms. The Hf orbitals are occupied as well, although only partially: most of the magnetization is localized in the interstitial space and in the vacancy cavity. The participation of Hf is clearly higher when its coordination number

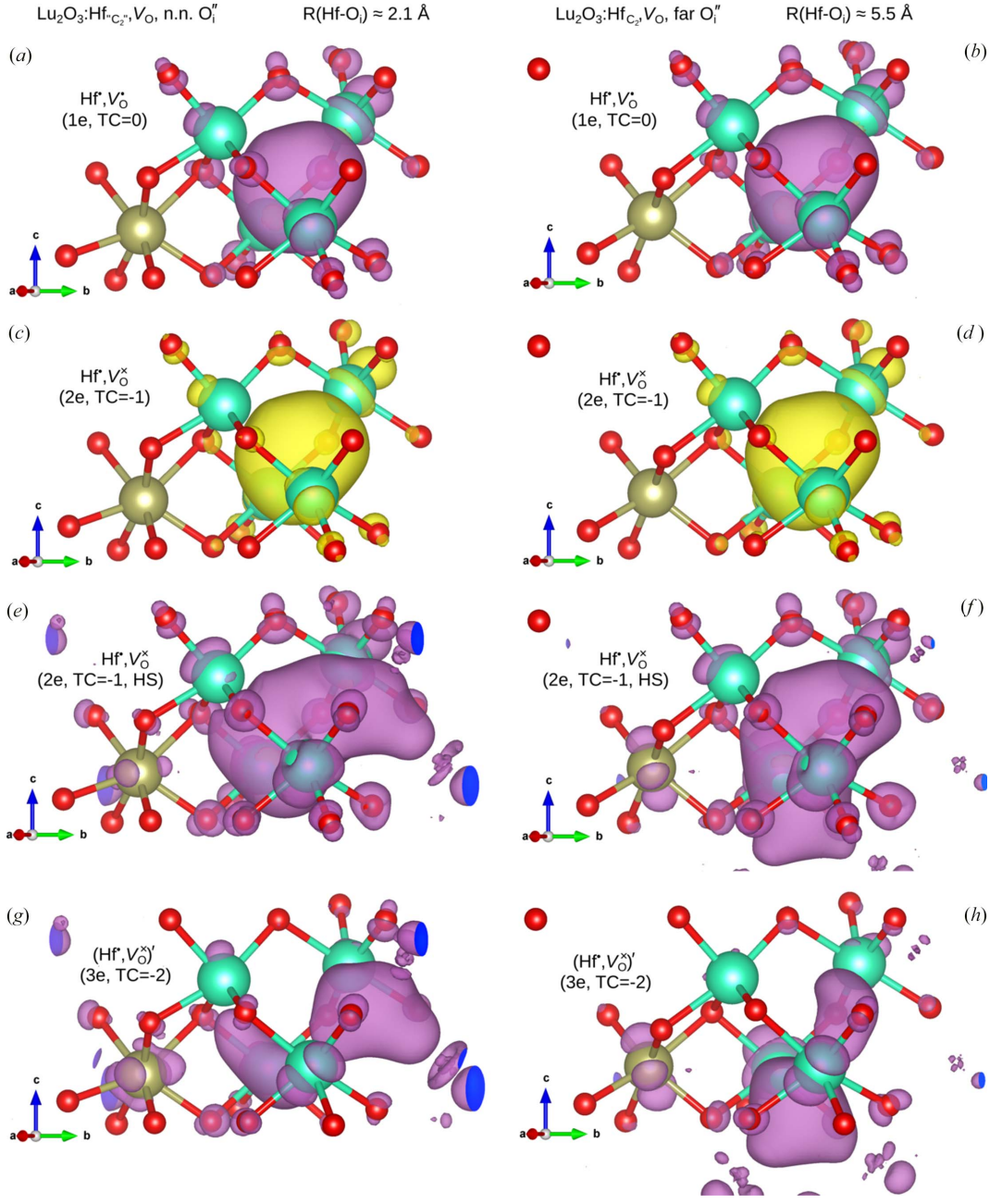


**Figure 6**
(*a*), (*b*), (*e*)–(*h*) Magnetization plots and (*c*) and (*d*) isosurface plots of the wavefunction corresponding to the trapped-electron KS eigenvalues at the Γ-point for $Lu_2O_3:Hf_{C_2}, V_O, O_i''$ with different numbers of additional/trapped electrons. The isosurface level is 0.0015. Lu atoms are turquoise, O atoms red, Hf golden.

is 6: the presence of an $O_i$ at Hf reduces its ability to accept electrons. This is in line with the findings in our previous work (Shyichuk & Zych, 2019; Shyichuk *et al.*, 2022), where it was shown that $O_i$ in the coordination environment disables electron trapping by Hf or Ta.

Finally, in the systems with three trapped electrons, the magnetization clearly avoids the location of the two-electron blob and tends to delocalize in the nearby interstitial cavities (voids), as well as at the nearby Lu atoms. The only case where that magnetization is localized at Hf is the $Lu_2O_3:Hf'_{C_{3i}}, V_O^{\times}, O_i''$ case. This finding is in line with previous work (Shyichuk *et al.*, 2022) where only $C_{3i}$ Hf dopants exhibited any electron trapping. The conclusion is also in line with the previous sections of the current paper: the same character of Hf participation was derived from the DOS plots.

Comparing the TD-DFT plots [Fig. 4(*h*)] with the electron localization data from Figs. 5 and 6, it can be concluded (again) that the absorption spikes correspond to $V_O^{\times} \rightarrow Hf^{\bullet}$ electron transfer, and this is also reflected in the correspondence between the spike transition energy and the respective energy difference in the DOS plots. The spike only occurs in cases where the electrons can localize at Hf, $Lu_2O_3:Hf'_{C_{3i}}, V_O^{\bullet}, O_i''$ in particular. In the other samples, localization is prevented by either the dopant being on the $C_2$ site, or the $O_i$ being in the direct neighborhood of the dopant. The relatively large transition intensity originates from its spatial character: the distance between the donor and the acceptor of the electron transfer is considerably larger than the size of an atom and the transition dipole must thus be large. The narrow band of the acceptor (Hf *d* orbital) is the factor explaining the small width of the spike.

### 3.5. Selected Zr counterparts

In Fig. 7, the DOS plots of the Zr-doped structures are overlapped with the respective DOS plots of Hf-doped structures. The latter were slightly shifted (by about 0.1 eV) for the best match. Despite the overall similarity, each of the sample pairs exhibits subtly different DOS plots. The biggest differences are in the bands of predominantly Zr and Hf character (as indicated by the respective dopant muffin-tin 5*d* contributions to the DOS plots, color-shaded in Fig. 7). The bands, however, are not occupied and consequently their impact on the electron trapping and de-trapping dynamics is questionable.

If the dopant metal is a part of the vacancy surroundings [Figs. 7(*a*) and 7(*b*)], the position of the respective vacancy band depends on the dopant: the Hf-doped samples exhibit slightly deeper vacancy-based electron traps. At the same time, the conduction-band edge does not depend on the dopant. Some contribution of the dopant 5*d* muffin-tin states to the vacancy band is visible. In the rest of the samples [Figs. 7(*c*)–7(*h*)], the vacancy bands exhibit almost no dependence on the dopant, and so does the conduction-band edge. Finally, in Fig. 7(*i*) DOS plots of $Lu_2O_3:M'_{C_{3i}}$ ($M$ = Zr, Hf) are shown. The two metal-based electron traps are both shallow and yet not identical (0.92 eV for Zr and 0.85 eV for Hf). Thus, if the electron trapping in $Lu_2O_3$:Hf and $Lu_2O_3$:Zr did happen in the form of locally formed $M^{3+}$, the corresponding glow curves would exhibit differences of about 10% in the trap depths. If a vacancy with dopant in its neighborhood acted as an electron trap, the differences in the glow curves should yet again correspond to something like a 5–10% difference in the trap depths. Finally, if vacancies with no dopant in their surroundings acted as electron traps, the differences in the glow curves would have been negligible. The latter conclusion is in line with experimental results indicating identical glow curves for Hf- and Zr-doped $Lu_2O_3$-based thermoluminescent ceramics (Sójka *et al.*, 2019).

A related phenomenon has recently been reported: metal-to-metal charge transfer (MMCT) barriers for Hf-to-Pr and Zr-to-Pr MMCTs in $Lu_2O_3$ [obtained using post-Hartree–Fock *ab initio* correlated calculations (Shyichuk & Krośnicki, 2023)] exhibited similar trends and similar yet different values. In other words, two different kinds of calculations on the same system (the referenced work and this work) indicate that Zr and Hf should exhibit non-identical trap parameters.

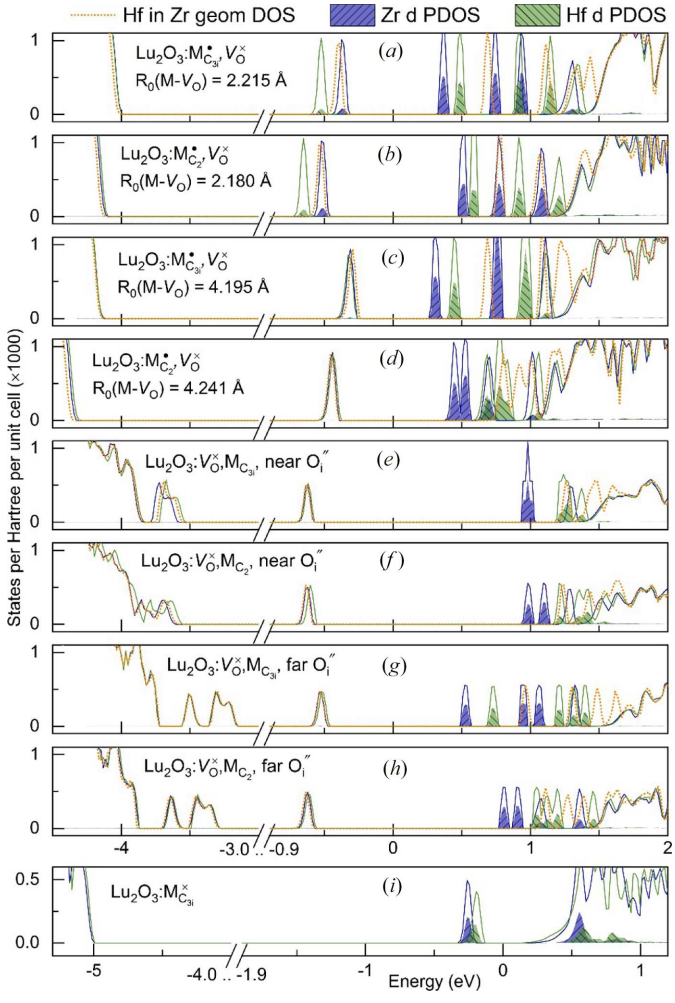


**Figure 7**
Comparison of DOS plots of selected $Lu_2O_3:M^{\times}$, $Lu_2O_3:M^{\bullet}, V_O^{\times}$ and $Lu_2O_3:M^{\bullet}, V_O^{\times}, O_i''$ systems. $M$ = Zr, Hf or Hf-in-Zr-geometry. The Fermi level is at zero. PDOS is partial (muffin-tin atomic) DOS.

Consequently, it is likely that $Lu_2O_3:Hf^{\bullet}/Zr^{\bullet}$, $V_O^{\bullet}$, $O_i''$ composite defects (a +4 metal dopant on the Lu site, a Frenkel pair, or an electron trapped on the vacancy site, so that another electron can be trapped and the summed charge is zero) are the main electron traps in $Lu_2O_3$:Hf/Zr. All three constituent impurities are probably not located in mutual proximity and thus behave as independent impurities, as reflected in the similarities between the glow curves of the Hf- and Zr-doped samples (Sójka *et al.*, 2019). The +4 dopant provides charge compensation for the electron present on the vacancy. The dopants must somehow promote the formation of Frenkel pairs, which is reflected in the fact that co-dopants are required to achieve efficient thermoluminescence in $Lu_2O_3$:Tb and $Lu_2O_3$:Pr.

To emphasize the differences between Zr and Hf in $Lu_2O_3$, a special set of calculations was performed: Hf dopant was placed instead of Zr in the optimized geometries of the Zr-doped samples. In other words, the calculations corresponded to an Hf dopant placed in the geometries corresponding to a Zr dopant. The respective DOS plots are shown as the orange dotted lines in Fig. 7. Interestingly, these plots correspond to neither Zr-doped nor Hf-doped sample DOS. The largest differences were in the empty bands of the predominantly dopant 5*d* character. The DOS plots of the Hf-in-Zr-geometry samples were more similar to the DOS of the Hf-doped samples than to those of the Zr-doped samples , at least in the part of the empty 5*d* bands. On the other hand, the vacancy band positions in the Hf-in-Zr-geometry samples were very similar to the respective positions in the Zr-doped sample DOS. The latter is true even for samples where the dopant is part of the vacancy environment [Figs. 7(*a*) and 7(*b*)]. In other words, the properties of electrons localized at *M* dopants are more affected by the dopant atomic properties, while vacancy-trapped electrons are mostly affected by the surrounding geometry. This conclusion is in line with the low participation of the atomic states in the vacancy band, and the fact that the respective electrons are mostly interstitial (Figs. 5 and 6). This is another argument against the electron-trapping mechanism in $Lu_2O_3$:Hf/Zr being the localized formation of the +3 dopant.

## 4. Conclusions

This work has analyzed the effects of a nearby Hf or Zr dopant on an oxygen vacancy electron trap in cubic $Lu_2O_3$. The only noticeable change in the oxygen vacancy trap depth occurs if the dopant is a part of the vacancy surroundings, *i.e.* if the vacancy site is surrounded by three Lu atoms and one *M* atom, *M* = Zr or Hf. The dopant atoms located further away exhibit minor effects on the oxygen vacancy trap depth, making it similar to the isolated vacancy trap depth or about 0.1 eV smaller.

Systems containing Zr or Hf dopant, an oxygen vacancy and an interstitial oxygen were analyzed as well. From a charge compensation point of view, a Frenkel pair accompanying the dopant is a reasonable option, as it corresponds to a lower total charge on the cell. In particular, the $Lu_2O_3:Hf^{\bullet}/Zr^{\bullet}$, $V_O^{\bullet}$, $O_i''$ system ($M^{4+}$, single electron trapped at the vacancy) is characterized by zero net charge and is capable of trapping another electron.

Introducing additional electrons to the latter system indicates that two electrons can be trapped at the vacancy site, while the third electron does not necessarily get trapped at Hf or Zr. Such trapping is possible, but it requires the dopant to be located on the $C_{3i}$ site. If the $O_i$ is bound to the dopant then the trapping properties of the dopant are disabled. The trap depth corresponding to the dopant in such a system is low, similar to that of the isolated Hf dopant (Shyichuk *et al.*, 2022). The oxygen vacancy electron traps are roughly twice as deep as the Zr/Hf-localized electron traps. The latter cannot provide permanent energy storage and are more likely to result in afterglow as the respective electron traps are rather shallow.

In this study, the distance between $Hf^{\bullet}$ and $V_O^{\bullet}$ centers in a c-$Lu_2O_3$ material was rather small, resulting in a strong preference of the trapped electron towards the vacancy site. If the distance was large, the two defects could potentially exhibit independent trapping and detrapping properties – afterglow and long-term energy storage, respectively. However, as the oxygen vacancy bands are lower in energy than the Zr/Hf 5*d* bands, the latter are unlikely to trap electrons if the empty or semi-occupied oxygen vacancy bands are present. The Zr/Hf localized traps would thus be the last to be occupied and the first to be emptied, in line with the presence of fading shallow traps in storage phosphors based on c-$Lu_2O_3$.

Optical stimulation of the trapped electrons was analyzed using time-dependent DFT. The trapped electron density can be excited to a localized state, while electron transfer to the dopant is also possible. The character of the preferred excited states is affected by the dopant site symmetry (preceding the introduction of other defects that might reduce it), the distance between the dopant and the vacancy, and the distance between the dopant and the interstitial oxygen. Thus, even if the Zr/Hf dopant was inactive as a trap, its presence might affect the dynamics of trap depopulation and the observed optical trap depth.

## Acknowledgements

Kevin F. Garrity from the National Institute of Standards and Technology (NIST, Maryland, USA) is acknowledged for providing the $Lu^{3+}$ pseudopotential. John K. Dewhurst from the Max Born Institute (Berlin, Germany) is acknowledged for his help at *Elk* forums. The Wrocław Center for Networking and Supercomputing is acknowledged for providing the necessary computing power (grant No. 300). Open-source software was used: *Elk* (https://elk.sourceforge.io), *Quantum Espresso* (https://www.quantum-espresso.org), Python (https://python.org), *Scipy* (https://scipy.org), *Inkscape* (https://inkscape.org/) and *LibreOffice* (https://www.libreoffice.org/).

## Funding information

The following funding is acknowledged: Narodowe Centrum Nauki (grant No. 2017/26/D/ST3/00599 to Andrii Shyichuk).

## References

Blaha, P., Schwarz, K., Tran, F., Laskowski, R., Madsen, G. K. H. & Marks, L. D. (2020). *J. Chem. Phys.*, **152**, 074101.
Bolek, P., Kulesza, D. & Zych, E. (2019). *J. Lumin.* **209**, 274–282.
Chen, S., Yang, Y., Zhou, G., Wu, Y., Liu, P., Zhang, F., Wang, S., Trojan-Piegza, J. & Zych, E. (2012). *Opt. Mater.* **35**, 240–243.
Dorenbos, P. (2017). *Opt. Mater.* **69**, 8–22.
Garrity, K. F., Bennett, J. W., Rabe, K. M. & Vanderbilt, D. (2014). *Comput. Mater. Sci.* **81**, 446–452.
Giannozzi, P., Andreussi, O., Brumme, T., Bunau, O., Buongiorno Nardelli, M., Calandra, M., Car, R., Cavazzoni, C., Ceresoli, D., Cococcioni, M., Colonna, N., Carnimeo, I., Dal Corso, A., de Gironcoli, S., Delugas, P., DiStasio, R. A., Ferretti, A., Floris, A., Fratesi, G., Fugallo, G., Gebauer, R., Gerstmann, U., Giustino, F., Gorni, T., Jia, J., Kawamura, M., Ko, H.-Y., Kokalj, A., Küçükbenli, E., Lazzeri, M., Marsili, M., Marzari, N., Mauri, F., Nguyen, N. L., Nguyen, H.-V., Otero-de-la-Roza, A., Paulatto, L., Poncé, S., Rocca, D., Sabatini, R., Santra, B., Schlipf, M., Seitsonen, A. P., Smogunov, A., Timrov, I., Thonhauser, T., Umari, P., Vast, N., Wu, X. & Baroni, S. (2017). *J. Phys. Condens. Matter*, **29**, 465901.
Giannozzi, P., Baroni, S., Bonini, N., Calandra, M., Car, R., Cavazzoni, C., Ceresoli, D., Chiarotti, G. L., Cococcioni, M., Dabo, I., Dal Corso, A., de Gironcoli, S., Fabris, S., Fratesi, G., Gebauer, R., Gerstmann, U., Gougoussis, C., Kokalj, A., Lazzeri, M., Martin-Samos, L., Marzari, N., Mauri, F., Mazzarello, R., Paolini, S., Pasquarello, A., Paulatto, L., Sbraccia, C., Scandolo, S., Sclauzero, G., Seitsonen, A. P., Smogunov, A., Umari, P. & Wentzcovitch, R. M. (2009). *J. Phys. Condens. Matter*, **21**, 395502.
Kröger, F. A. & Vink, H. J. (1956). *Solid State Physics*, Vol. 3, edited by F. Seitz & D. Turnbull, pp. 307–435. Cambridge, Massachusetts, USA: Academic Press.
Kulesza, D., Bolek, P., Bos, A. J. J. & Zych, E. (2016). *Coord. Chem. Rev.* **325**, 29–40.
Kulesza, D., Bos, A. J. J. & Zych, E. (2018). *J. Alloys Compd.* **769**, 794–800.
Kulesza, D., Trojan-Piegza, J. & Zych, E. (2010). *Radiat. Meas.* **45**, 490–492.
Kulesza, D., Wiatrowska, A., Trojan-Piegza, J., Felbeck, T., Geduhn, R., Motzek, P., Zych, E. & Kynast, U. (2013). *J. Lumin.* **133**, 51–56.
Kulesza, D. & Zych, E. (2013). *J. Phys. Chem. C*, **117**, 26921–26928.
Perdew, J. P. & Zunger, A. (1981). *Phys. Rev. B*, **23**, 5048–5079.
Petermann, K., Fornasiero, L., Mix, E. & Peters, V. (2002). *Opt. Mater.* **19**, 67–71.
Räsänen, E., Pittalis, S. & Proetto, C. R. (2010). *J. Chem. Phys.* **132**, 044112.
Sharma, S., Dewhurst, J. K., Sanna, A. & Gross, E. K. U. (2011). *Phys. Rev. Lett.* **107**, 1–5.
Sharma, S., Dewhurst, J. K., Sanna, A., Rubio, A. & Gross, E. K. U. (2012). *New J. Phys.* **14**, 053052.
Shyichuk, A. & Krośnicki, M. (2023). *J. Phys. Chem. A*, **127**, 4583–4595.
Shyichuk, A., Kulesza, D. & Zych, E. (2022). *Acta Cryst.* B**78**, 564–575.
Shyichuk, A. & Zych, E. (2019). *J. Lumin.* **214**, 116583.
Shyichuk, A. & Zych, E. (2020). *J. Phys. Chem. C*, **124**, 14945–14962.
Sójka, M., Kulesza, D., Bolek, P., Trojan-Piegza, J. & Zych, E. (2019). *J. Rare Earths*, **37**, 1170–1175.
Trojan-Piegza, J., Zych, E., Hölsä, J. & Niittykoski, J. (2009). *J. Phys. Chem. C*, **113**, 20493–20498.
Wiatrowska, A. & Zych, E. (2012). *2012 IEEE International Conference on Oxide Materials for Electronic Engineering (OMEE)*, 3–7 September 2012, Lviv, Ukraine, pp. 247–248. New York: IEEE.
Wiatrowska, A. & Zych, E. (2013*a*). *Materials*, **7**, 157–169.
Wiatrowska, A. & Zych, E. (2013*b*). *J. Phys. Chem. C*, **117**, 11449–11458.
Wimmer, E., Krakauer, H., Weinert, M. & Freeman, A. J. (1981). *Phys. Rev. B*, **24**, 864–875.
Zeler, J., Jerzykiewicz, L. & Zych, E. (2014). *Materials*, **7**, 7059–7072.
Zych, E., Bolek, P. & Kulesza, D. (2017). *J. Lumin.* **189**, 153–158.
Zych, E. & Kulesza, D. (2014). *Z. Naturforsch. Teil B*, **69**, 165–170.